Rechargeable Aqueous Zinc-Ion Battery Based on Porous Framework Zinc Pyrovanadate Intercalation Cathode

Chuan Xia, Jing Guo, Yongjiu Lei, Hanfeng Liang, Chao Zhao, and Husam N. Alshareef*

In this work, a microwave approach is developed to rapidly synthesize ultra-long zinc pyrovanadate ($Zn_3V_2O_7(OH)_2 \cdot 2H_2O$, ZVO) nanowires with a porous crystal framework. It is shown that our synthesis strategy can easily be extended to fabricate other metal pyrovanadate compounds. The zinc pyrovanadate nanowires show significantly improved electrochemical performance when used as intercalation cathode for aqueous zinc–ion battery. Specifically, the ZVO cathode delivers high capacities of 213 and 76 mA h g^{-1} at current densities of 50 and 3000 mA g^{-1}, respectively. Furthermore, the Zn//ZVO cells show good cycling stability up to 300 cycles. The estimated energy density of this Zn cell is ≈214 Wh kg^{-1}, which is much higher than commercial lead–acid batteries. Significant insight into the Zn-storage mechanism in the pyrovanadate cathodes is presented using multiple analytical methods. In addition, it is shown that our prototype device can power a 1.5 V temperature sensor for at least 24 h.

Cost-effective, environmentally friendly, and reliable energy storage is critical for widespread utilization of renewable energy sources.[1,2] Even though lithium intercalation cells with high energy density have clearly dominated our daily life, they still face challenges to scale up for large-scale applications, such as grid-level storage. This limitation is due to the cost, safety, lifespan, and toxicity of the Li cell components. The desire to achieve a truly sustainable future has brought significant attention to aqueous rechargeable batteries, especially for stationary grid-level storage of renewable energies,[3] where fast-response-balancing systems for frequency regulation are crucial.[2,4] This is because aqueous electrolytes offer much higher ionic conductivities (≈1 S cm^{-1}) compared to nonaqueous electrolytes (≈1–10 mS cm^{-1}), which favors high-rate capabilities.[5] More importantly, the aqueous rechargeable batteries (such as lead–acid system) are much safer, cheaper, and easier to scale up than organic Li-ion cells. These characteristics are particularly important in stationary applications, where operational safety and low cost are more important than weight.[3,5] While the lead–acid batteries account for more than half of the global battery market, the use of toxic lead with their limited energy and

lifetime means that alternative solutions are needed.

Many types of aqueous rechargeable batteries using multivalent metal ions (e.g., Zn^{2+}, Mg^{2+}, and Al^{3+}) as charge carriers have been proposed.[6–8] This is because rechargeable cells employing multivalent ions can, in principle, deliver higher storage capacity due to multiple electron transfers. Among them, intercalation chemistry based on Zn^{2+} ions in aqueous Zn-ion batteries (ZIBs) is particularly promising thanks to the high Zn metal anode capacity (820 mA h g^{-1}).[9] In addition, Zn offers several attractive attributes including low cost (USD $2 kg^{-1}),[5] high electrical conductivity,[10] nontoxicity,[11] easy processing, and a more suitable redox potential (–0.76 V vs standard hydrogen electrode) in aqueous electrolyte.[10] Further, previous studies have demonstrated that dendritic zinc issues, while prevalent in alkaline electrolytes, are virtually eliminated using neutral (or slightly acidic) pH electrolyte,[5] making the aqueous ZIBs attractive from a safety standpoint. Aqueous ZIB was first introduced by Kang and co-workers,[7] where tunnel-type MnO_2 was used as cathode in 1 M $ZnSO_4$ or $Zn(NO_3)_2$ aqueous electrolyte. After this pioneering demonstration, only Prussian blue analogs (ZnHCF[12] and CuHCF[13,14]) and polymorphous of MnO_2[15] were seriously investigated as potential Zn^{2+} ion host materials, but they suffer from either limited capacity (≈50 mA h g^{-1}) or very poor cycling stability. Hence, the development of stable ZIB cathode with higher energy density is crucial to realize aqueous ZIBs for large-scale energy storage.

Very recently, layered and tunnel-type vanadium-based compounds ($Zn_{0.25}V_2O_5 \cdot nH_2O$,[5] LiV_3O_8,[8] $Na_3V_2(PO_4)_3$,[10] VS_2,[16] and $VO_{1.52}(OH)_{0.77}$[17]) have been reported as potential cathode materials for aqueous ZIBs. The reported performance improvements were attributed mainly to their open-framework crystal structure and the tendency of vanadium to exist in multiple oxidation states. To capitalize on these features, herein, we have developed a microwave approach to rapidly synthesize ultralong zinc pyrovanadate ($Zn_3V_2O_7(OH)_2 \cdot 2H_2O$ or ZVO) nanowires with a porous crystal framework (**Figure 1**A), which can facilitate the electrochemical (de)intercalation of Zn^{2+} ions into the ZVO lattice. We demonstrate that the ZVO cathode can deliver high capacities of 213 and 76 mA h g^{-1} at current densities of 50 and 3000 mA g^{-1}, respectively. Further, we show that the Zn^{2+} ion uptake/removal process occurs without porous-framework collapse, suggesting that ZVO anodes synthesized

C. Xia, J. Guo, Y. Lei, Dr. H. Liang, Dr. C. Zhao, Prof. H. N. Alshareef
Materials Science and Engineering
King Abdullah University of Science and Technology (KAUST)
Thuwal 23955-6900, Saudi Arabia
E-mail: husam.alshareef@kaust.edu.sa

The ORCID identification number(s) for the author(s) of this article can be found under https://doi.org/10.1002/adma.201705580.
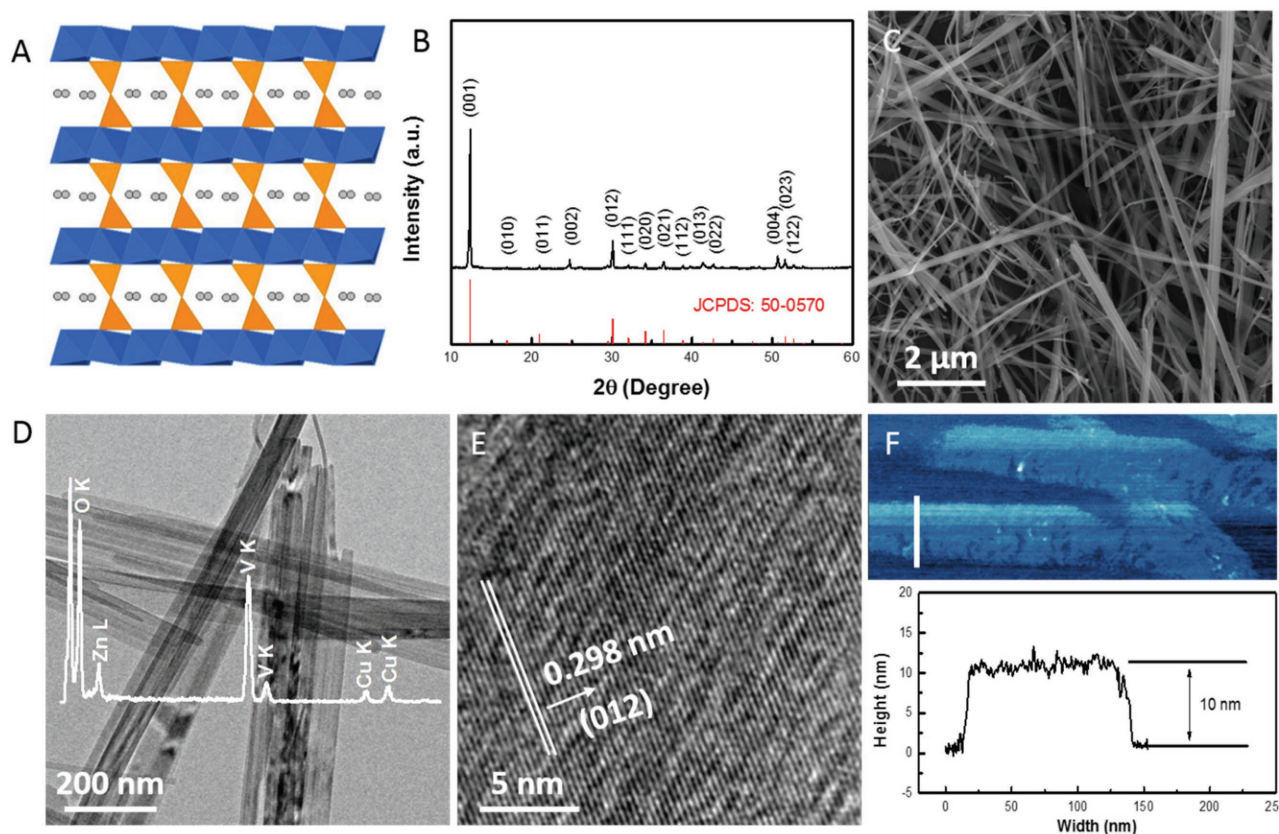
Figure 1. Structural characterizations of as-synthesized ZVO nanowires. A) Crystal structure viewed along the *b*-axis of ZVO, which shows a layered structure with porous framework. The Zn atoms in ZnO_6 and V atoms in V_2O_7 polyhedra are depicted in blue and yellow, respectively. The gray atoms in the crystal cavities represent the lattice water. B) Typical θ–2θ XRD pattern of ZVO nanowires. C–E) SEM, TEM, and high-resolution TEM images of ZVO nanowires. Inset in (D) shows the EDS spectrum of as-obtained ZVO, showing the existence of O, Zn, and V elements. F) AFM images of an individual ZVO nanowire, revealing an average thickness of ≈10 nm.

by the simple microwave process is indeed a potential Zn^{2+} host in aqueous ZIBs.

Zinc pyrovanadate crystallizes in the trigonal system ($P\overline{3}m1$), and its structure is built up of zinc oxide layers separated by V–O–V pillars ($V_2O_7^{4-}$ group) (Figure 1A). The brucite type of layer is formed by close-packed terminal O atoms of pyrovanadate and hydroxide groups. The Zn atoms occupy three of four octahedral sites in a close-packed layer of O atoms.[18] The water molecules randomly fill in the large cavities. Such an open-framework and expanded interlayer spacing (0.719 nm vs 0.576 nm of VS_2) offer a good possibility for electrochemical insertion/extraction of Zn^{2+} ions. Moreover, our microwave approach is more appealing than traditional hydrothermal processes because it enables rapid synthesis and higher yield. More importantly, we show that this microwave technique can easily be extended to fabricate other metal pyrovanadate, e.g., $Cu_3V_2O_7(OH)_2\cdot2H_2O$ (Figure S1, Supporting Information). The XRD pattern of as-prepared product is shown in Figure 1B. It is clear that all the diffraction peaks can be indexed to $Zn_3V_2O_7(OH)_2\cdot2H_2O$ (JCPDS 50-0570), indicating that single-phase ZVO has been formed. It is interesting to note that the XRD intensity ratio $I(001)/I(012)$ of the ZVO prepared by our process shows a dramatic enhancement in comparison to hydrothermally synthesized ZVO nanosheets,[19] nanoplates,[20]

and microflowers.[21] Moreover, the preferential orientation of ZVO made by our process along the [001] direction (*c*-axis) may provide better access for guest Zn^{2+} ions into the available sites. The typical nanowire morphology of as-prepared ZVO is shown in the scanning electron microscope (SEM) and transmission electron microscope (TEM) images of Figure 1C,D and Figure S2 (Supporting Information), which show the nanowires to be tens of micrometers long and ≈100 nm wide. The energy-dispersive X-ray spectroscopy (EDS) analysis (inset in Figure 1D) also confirms the purity of the ZVO nanowires. A lattice fringe with *d*-spacing of 0.298 nm can be observed in the high-resolution TEM image, corresponding to (012) plane of ZVO nanowire (Figure 1E). In addition, we show that the ZVO nanowires are ≈10 nm thick, as determined by atomic force microscopy (Figure 1F; Figure S3, Supporting Information). It is believed that these morphological features can effectively shorten the diffusion pathway of Zn^{2+} ions in ZVO, thus enhancing its rate behavior.

Under the galvanostatic condition of 50 mA g^{-1} current density, the electrochemical profiles representing Zn^{2+} (de)intercalation into ZVO host are presented in **Figure 2**A. The discharge and charge plateau-like regions which are located, respectively, at 0.85/0.58 and 0.74/1.0 V are obviously observed in the second and third charge–discharge (CD) cycles, which probably
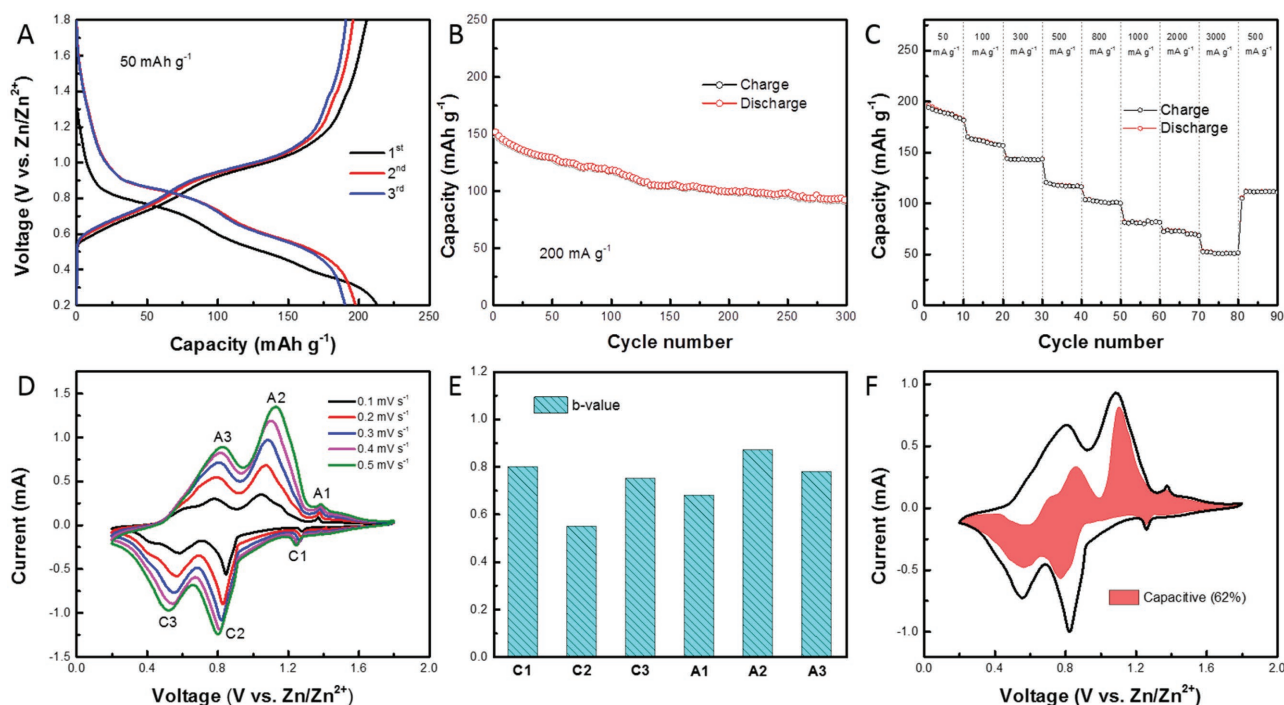
Figure 2. Electrochemical performance of the ZVO cathodes. A) Galvanostatic charge–discharge profiles for ZVO electrodes at a current density of 50 mA g^{-1}. B) Cycle performance at a current rate of 200 mA g^{-1}. C) Rate capability of the ZVO cathode. D) Cyclic voltammetry curves at different scan rates. E) The *b*-values of different redox peaks, determined from the log(i) versus log(v) plots. F) The k_1 analysis of ZVO electrode at 0.3 mV s^{-1}. These data show the contribution to capacitive charge storage as a function of potential.

correspond to the insertion/extraction of Zn^{2+} ions from ZVO crystal. A very high discharge capacity of 213 mA h g^{-1} is initially obtained in the first cycle, corresponding to an ≈3.8 electron redox process, of which 205 mA h g^{-1} is recovered upon charging. Figure 2B shows the cycling performance of Zn//ZVO cell at an average voltage of ≈1.33 V (vs Zn/Zn^{2+}). Note that for the estimation of the average voltage, the integral of the voltage–charge curve was divided by the total charge.[13] The battery delivers a reversible capacity of 101 mA h g^{-1} (68%) after 300 cycles and the Coulombic efficiency approaches >96% in all cycles. It is worthwhile to note that a rapid capacity degradation occurs in the initial 30 cycles. We attribute this abrupt capacity fading to the formation of byproducts on the ZVO surface which may have been decomposed by the ZnSO$_4$ electrolyte,[17] as discussed later. However, the formation of surface sulfate suppresses further dramatic capacity fading. This process is consistent with the reduced amount of capacity fading in the subsequent cycles, and hence, a stabilized capacity was observed over hundreds of cycles (100th to 300th cycles). The good rate capability of ZVO cathode is illustrated in Figure 2C, where the current density was increased stepwise from 50 to 3000 mA g^{-1} and returned to 500 mA g^{-1}. The discharge capacities at 50, 100, 300, 500, 800, 1000, 2000, and 3000 mA g^{-1} are ≈200, 166, 145, 122, 105, 84, 75, and 54 mA h g^{-1}, respectively. Impressively, when the current density was returned to 500 mA g^{-1}, the discharge capacity recovered to 112 mA h g^{-1}, suggesting only a slight structural modification of ZVO during intense current fluctuation.

Cyclic voltammetry (CV) measurements were performed to further investigate the Zn-ion storage behavior of the ZVO
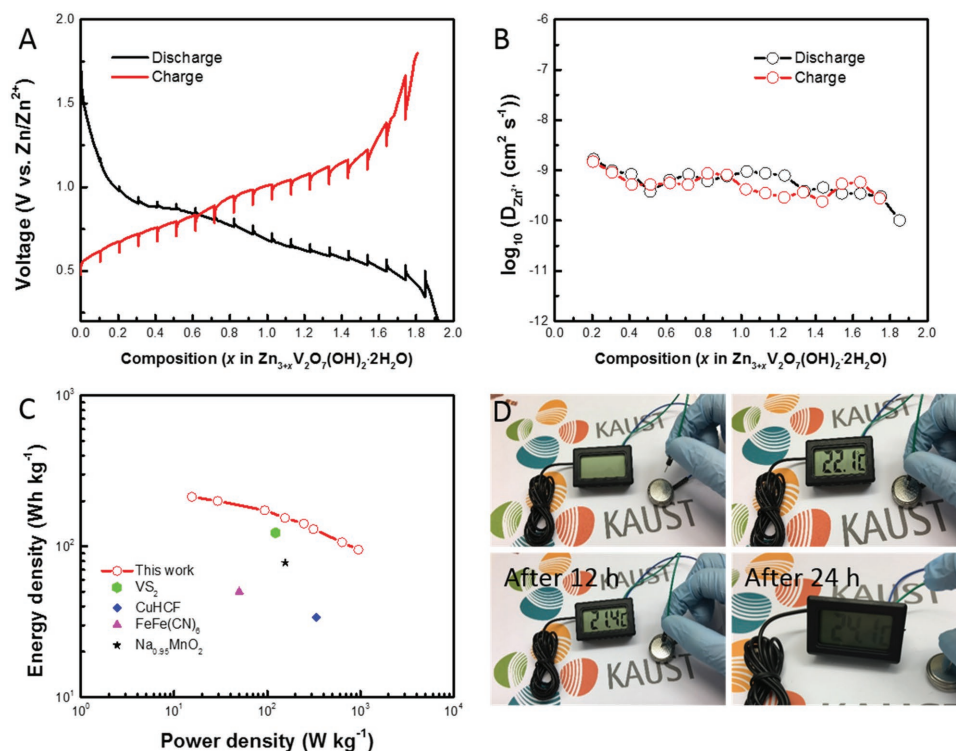
nanowires. Figure 2C exhibits representative CV curves of the ZVO cathode measured at diffident scan rates. The three distinct pairs of peaks at around 1.28/1.37 V (C1/A1), 0.84/1.05 V (C2/A2), and 0.58/0.79 V (C3/A3) can be attributed to a three-step reaction associated with Zn^{2+} ion intercalation and extraction through the ZVO lattice, which are in agreement with previous reports.[22] For instance, two pairs of reduction/oxidation peaks located at 0.8/1.1 and 0.65/0.79 V are observed for LiV$_3$O$_8$ when used as cathodes for ZIBs.[8] Furthermore, with the continuous increase of the scan rates from 0.1 to 0.5 mV s^{-1}, the CV profiles retain their shapes, showing the good stability of ZVO cathodes. To further understand the charge storage kinetics in the ZVO host, we quantitatively separated the diffusion-controlled and capacitive contributions to the measured current using sweep voltammetry.[23] Generally, the relationship between the measured peak current (i) and sweep rate (v) in a CV scan can be described by the following equation

$$i = av^b \qquad (1)$$

A *b* value of 0.5 indicates that the current is controlled by semiinfinite diffusion, while *b* = 1 indicates capacitive behavior.[24] For ZVO, the *b*-values of the six peaks are 0.8, 0.55, 0.75, 0.68, 0.87, and 0.78 (Figure 2D), indicating mainly capacitor-like kinetics. We also quantitatively separated the diffusion-controlled and capacitive contributions using an analysis where the current response, i (V), is assumed to be a combination of capacitor-like and diffusion-controlled processes

$$i(V) = k_1 v + k_2 v^{1/2} \qquad (2)$$

ADVANCED
SCIENCE NEWS
www.advancedsciencenews.com

ADVANCED
MATERIALS
www.advmat.de

Figure 3. Performance assessment of the Zn/ZVO cell. A) Charge–discharge GITT curves for the ZVO cathode at a current density of 30 mA g^{-1}, and B) the corresponding Zn^{2+} coefficients as a function of the Zn^{2+} composition during CD scan of the ZVO cathode. C) The Ragone plot of Zn//ZVO cell, in comparison with other aqueous ZIBs (Zn//VS$_2$ (ref. [16]), Zn//CuHCF (ref. [13]), Zn//FeFe(CN)$_6$ (ref. [30]), and Zn//Na$_{0.95}$MnO$_2$ (ref. [31])). D) Digital image of a 1.5 V temperature sensor powered by two Zn/ZVO cells in series.

By determining k_1, it is possible to estimate, as a function of potential, the fraction of current contributed by capacitor-like processes.[23] As shown in Figure 2E, 62% of the current can be attributed to the capacitive response at a scan rate of 0.3 mV s^{-1}, which is responsible for high-rate capability of the cell. Additionally, the galvanostatic intermittent titration technique (GITT) was employed to calculate the Zn^{2+} ion diffusion coefficient in ZVO cathode (**Figure 3**A,B, see details in Note S2 in the Supporting Information). Despite the divalent nature of the Zn^{2+} ion, the GITT-determined diffusion coefficient is ≈10^{-9} to 10^{-10} cm^2 s^{-1}, which is 10^2–10^4 higher than the Li$^+$ diffusion in LiFePO$_4$,[25] Li$_3$V$_2$(PO$_4$)$_3$,[26] LiV$_3$O$_8$,[27] TiO$_2$,[28] and LiCoO$_2$[29] in organic or aqueous cells. This result clearly shows that the open-framework structure of the ZVO cathode allows fast Zn^{2+} immigration, leading to good rate capabilities. The high-rate performance of our Zn//ZVO cell is compared to other reported Zn^{2+} ion cells as shown in the Ragone plot (Figure 3C). It can be seen that our cells offer better performance than cells based on CuHCF,[13] VS$_2$,[16] FeFe(CN)$_6$,[30] and Na$_{0.95}$MnO$_2$[31] cathodes. To visually illustrate the potential of this Zn cell for practical applications, we show that our prototype device (two cells in series) can power a 1.5 V temperature sensor (1.5 V, 0.15 mW) for at least 24 h (Figure 3D).

In order to gain insight into the electrochemical intercalation process in the ZVO host, ex situ XRD analysis was carried out. Figure S4A (Supporting Information) shows that Bragg peaks corresponding to ZVO phase shift to lower angles in the fully discharged state (0.2 V) in the first cycle, and nearly return to
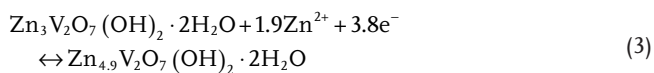
their initial positions upon discharging to 1.8 V. Interestingly, the ZVO electrode preserves its crystal structure after 100 continues CD cycles (Figure S4B, Supporting Information), indicating highly reversible Zn^{2+} intercalation of ZVO host without breakdown of its porous framework. It is worth noting that the formation of Zn$_4$SO$_4$(OH)$_6$·4H$_2$O byproduct due to the reaction with the electrolyte was observed after the first discharge (Figure S4A, Supporting Information). This result is probably responsible for the abrupt capacity fading at the initial cycles. However, most of the basic zinc sulfate byproduct was diminished after subsequent charging process. Furthermore, we did not observe any impurity signals from XRD analysis after 100 CD cycles (Figure S4B, Supporting Information), which is consistent with the significantly reduced trend in capacity fading in the subsequent cycles. **Figure 4**A displays the evolution of the (001) peak of ZVO electrode in detail during the second CD scan. Upon continues voltage increase, the (001) peak gradually shifts from 12.58° to 12.26°, revealing an interlayer expansion process of the brucite-type layer, which can be immediately recovered upon voltage reversal. This reversibility and gradual shifting of the (001) peak confirms that the related process is associated with Zn^{2+} uptake/removal from ZVO lattice. It is worth noting a small amount of Zn^{2+} may have remained trapped in the crystal structure which caused less than 100% recovery of the (001) peak from 0.2 to 1.8 V at the second cycle. This phenomenon is likely another reason that contributes to the gradual capacity fading. The ex situ high-resolution TEM analysis (Figure 4B) also shows reversible changes of the
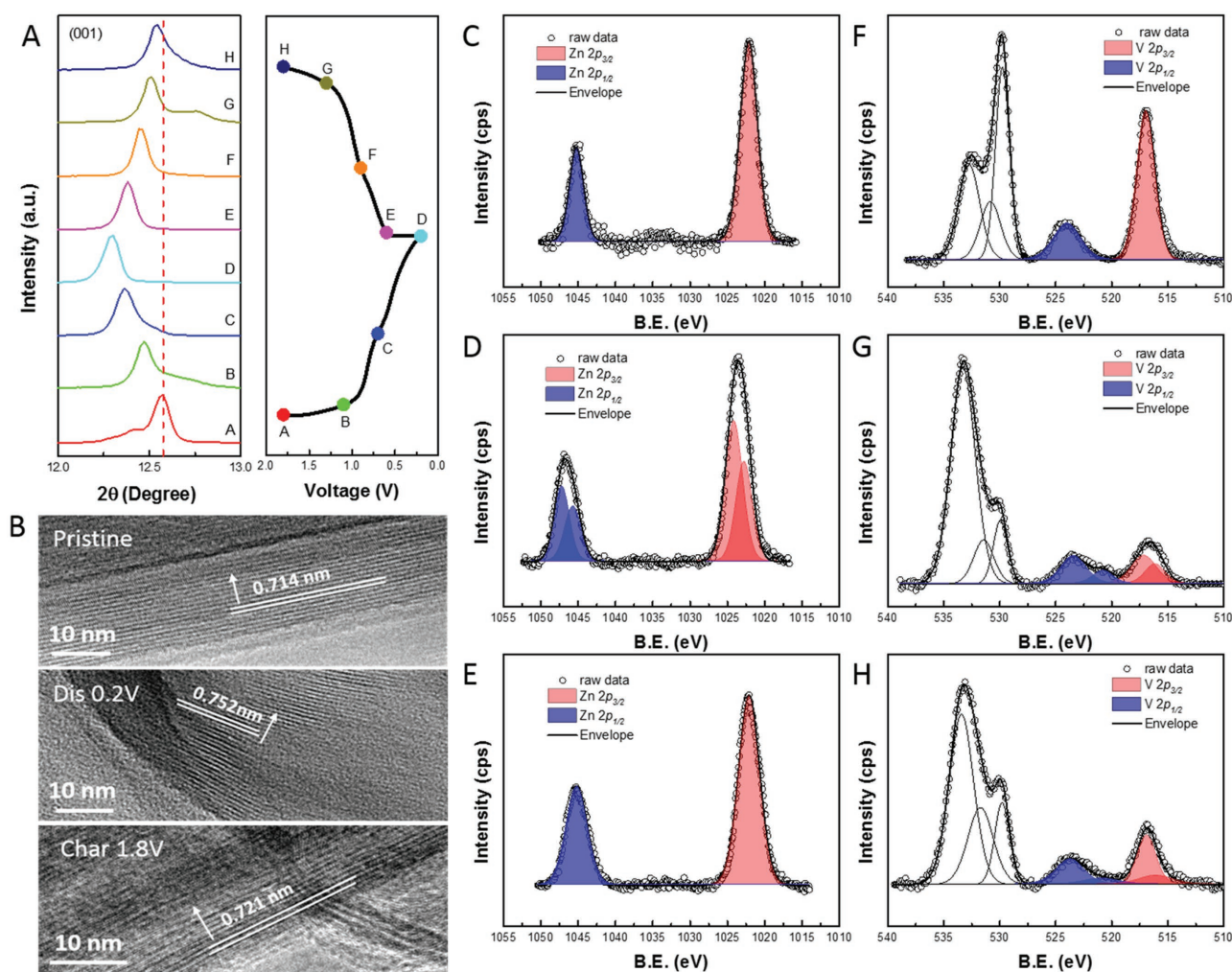
Figure 4. Analysis of the Zn-storage mechanism in ZVO cathode. A) Ex situ XRD patterns of (001) Bragg peak of the ZVO electrode during second charge–discharge scan as a function of discharge and charge voltage. B) High-resolution TEM of the ZVO nanowire at initial, fully discharged (0.2 V) and charged (1.8 V) state. Ex situ high-resolution XPS spectra of the C–E) Zn 2p and F–H) V 2p regions in pristine, fully discharged, and charged state of the ZVO electrodes.

lattice spacing of the ZVO (001) plane during the second cycle, which is consistent with the XRD study and also supports the reversible intercalation reaction mechanism. These results were subsequently substantiated by ex situ X-ray photoelectron spectroscopy (XPS) analysis. The pristine (Figure 4C) and fully charged (Figure 4E) ZVO electrodes show only one Zn 2p ($2p_{3/2}$: 1022 eV)[32] component due to the native Zn^{2+} sites in the ZVO lattice. However, in fully discharged state (Figure 4D), we observe a second Zn contribution where the Zn $2p_{3/2}$ peak is located at 1024 eV, which corresponds to the intercalated Zn in ZVO. In addition, reversible electrochemical reduction of V–O–V pillars as a consequence of Zn^{2+} insertion is also evident in the V 2p XPS region. The peak fitting analysis of the pristine ZVO electrode shows that its V $2p_{3/2}$ peak is located at 517 eV (Figure 4F), corresponding to V^{5+} species.[33] When discharging to 0.2 V, another V $2p_{3/2}$ feature appears (Figure 4G), indicating partial reduction of V^{5+} to $V^{\delta+}$ ($\delta < 5$). As shown in Figure 4H, the $V^{\delta+}$ contribution is almost diminished upon charging (for detailed discussion see Note S3 in the Supporting

Information), confirming the reversibility and stability of the ZVO crystal. Based on the above discussions, the electrochemical reaction of Zn//ZVO cell at current density of 50 mA g^{-1} can be described using the following equations

$$Zn_3V_2O_7(OH)_2 \cdot 2H_2O + 1.9Zn^{2+} + 3.8e^- \\ \leftrightarrow Zn_{4.9}V_2O_7(OH)_2 \cdot 2H_2O \tag{3}$$

$$Zn^{2+} + 2e^- \leftrightarrow Zn \tag{4}$$

Considering the low cost of both Zn (≈USD $2 kg^{-1}) and V (≈USD $2.5 lb^{-1}),[5] the combination of a high-capacity, dendrite-free Zn anode and a stable ZVO cathode in a mild aqueous electrolyte presents a potentially safe, durable, and cost-efficient device for large-scale energy storage.

In summary, we report a simple microwave approach to synthesize layered metal pyrovanadate nanowires ($Zn_3V_2O_7(OH)_2 \cdot 2H_2O$ or ZVO) as cathodes for ZIBs in aqueous electrolyte. The ZVO cathode delivers high capacities

**ADVANCED
SCIENCE NEWS**
www.advancedsciencenews.com

**ADVANCED
MATERIALS**
www.advmat.de

of 213 and 76 mA h g^{-1} at current densities of 50 and 3000 mA g^{-1}, respectively. Excellent rate behavior was demonstrated, and the Zn//ZVO cells show good cycling stability up to 300 cycles. The estimated energy density of our Zn cell is ≈214 Wh kg^{-1} which is much higher than commercial lead–acid batteries. Mechanistic details of the Zn-storage mechanism based on Zn^{2+} ions intercalation were elucidated. The high capacity, low cost, and safety make our devices promising for stationary grid storage applications.

Experimental Section

Synthesis of Ultralong Zn$_3$V$_2$O$_7$(OH)$_2$·2H$_2$O Nanowire: In a typical synthesis, 1.5 mol commercial Zn(NO$_3$)$_2$·2H$_2$O was first dissolved in 20 mL deionized (DI) water. Then, 1.0 mol commercial NH$_4$VO$_3$ powders were added into another 20 mL DI water and stirred at 80 °C for 10 min to form a homogeneous yellow solution. Next, the above NH$_4$VO$_3$ solution was dropwise added to the zinc solution and stirred for 5 min. The above homogenous solution was transferred to a sealed glass vessel and placed in a CEM Discover SP microwave synthesis system. The system temperature was raised to 180 °C in 2 min and maintained for 6 h. After cooling, the as-synthesized product was collected and rinsed with ethanol and DI, and dried in a vacuum at 60 °C for 24 h.

Structural Characterization: The as-synthesized samples were characterized using a Bruker D8 ADVANCE X-ray diffractormeter (XRD) using Cu Kα radiation (λ = 1.5406 Å), an FEI Nova Nano 630 scanning electron microscope, and an FEI Titan 80-300 ST (300 kV) transmission electron microscope with energy dispersive X-ray spectroscopy capabilities. X-ray photoelectron spectroscopy measurements were performed using a Kratos Axis Ultra DLD spectrometer with Al Kα radiation ($h\nu$ = 1486.6 eV). All XPS spectra were calibrated by shifting the detected adventitious carbon C 1s peak to 284.4 eV. Atomic force microscopy (AFM) images were recorded using a Digital Instrument Multi-Mode AFM with a Nanoscope 4 controller operating in tapping mode.

Zn-Ion Battery Performance Measurement: To assess the battery performance, 2032 coin-type (MTI, Inc.) devices were fabricated. Self-supported Zn$_3$V$_2$O$_7$(OH)$_2$·2H$_2$O membrane was fabricated using a vacuum filtration method to serve as the working electrode. Typically, zinc pyrovanadate nanowires were mixed with conducting Super P and a water-based composite binder (carboxymethylcellulose) and styrene–butadiene rubber in a 70:27:2:1 weight ratio. The composite film was punched into ≈1 cm^{-2}, and the active material mass loading is around 4–5 mg cm^{-2}. Zinc foil was used as the counter and reference electrode, and Celgard 3501 microporous membrane as separator. 1 M ZnSO$_4$ in water was used as electrolyte. Stainless steel was used as current collector. The electrochemical performance of the assembled cells was measured at different current densities in the voltage window from 0.2 to 1.8 V versus Zn/Zn^{2+} using an Arbin battery tester (Arbin BT-2143-11U, College Station, TX, USA). Cyclic voltammetry was performed to examine the reduction and oxidation peaks in the voltage range of 0.2–1.8 V versus Zn/Zn^{2+} at a scan rate of 0.1–1 mV s^{-1} using VMP3 Biologic potentiostat (Biologic, France).

Supporting Information

Supporting Information is available from the Wiley Online Library or from the author.

Acknowledgements

Conflict of Interest

The authors declare no conflict of interest.

Keywords

[1] a) P. Simon, Y. Gogotsi, B. Dunn, *Science* **2014**, *343*, 1210; b) M. Armand, J. M. Tarascon, *Nature* **2008**, *451*, 652.

[2] B. Dunn, H. Kamath, J.-M. Tarascon, *Science* **2011**, *334*, 928.

[3] J. O. G. Posada, A. J. Rennie, S. P. Villar, V. L. Martins, J. Marinaccio, A. Barnes, C. F. Glover, D. A. Worsley, P. J. Hall, *Renewable Sustainable Energy Rev.* **2017**, *68*, 1174.

[4] C. D. White, K. M. Zhang, *J. Power Sources* **2011**, *196*, 3972.

[5] D. Kundu, B. D. Adams, V. Duffort, S. H. Vajargah, L. F. Nazar, *Nat. Energy* **2016**, *1*, 16119.

[6] a) M. Pasta, C. D. Wessells, R. A. Huggins, Y. Cui, *Nat. Commun.* **2012**, *3*, 1149; b) Z. Li, K. Xiang, W. Xing, W. C. Carter, Y. M. Chiang, *Adv. Energy Mater.* **2015**, *5*, 1401410; c) C. D. Wessells, R. A. Huggins, Y. Cui, *Nat. Commun.* **2011**, *2*, 550.

[7] C. Xu, B. Li, H. Du, F. Kang, *Angew. Chem. Int. Ed.* **2012**, *51*, 933.

[8] M. H. Alfaruqi, V. Mathew, J. Song, S. Kim, S. Islam, D. T. Pham, J. Jo, S. Kim, J. P. Baboo, Z. Xiu, *Chem. Mater.* **2017**, *29*, 1684.

[9] J. F. Parker, C. N. Chervin, I. R. Pala, M. Machler, M. F. Burz, J. W. Long, D. R. Rolison, *Science* **2017**, *356*, 415.

[10] G. Li, Z. Yang, Y. Jiang, C. Jin, W. Huang, X. Ding, Y. Huang, *Nano Energy* **2016**, *25*, 211.

[11] X. G. Zhang, *Corrosion and Electrochemistry of Zinc*, Springer Science & Business Media, New York **2013**.

[12] L. Zhang, L. Chen, X. Zhou, Z. Liu, *Adv. Energy Mater.* **2015**, *5*, 1400930.

[13] R. Trócoli, F. La Mantia, *ChemSusChem* **2015**, *8*, 481.

[14] Z. Jia, B. Wang, Y. Wang, *Mater. Chem. Phys.* **2015**, *149*, 601.

[15] a) H. Pan, Y. Shao, P. Yan, Y. Cheng, K. S. Han, Z. Nie, C. Wang, J. Yang, X. Li, P. Bhattacharya, *Nat. Energy* **2016**, *1*, 16039; b) M. H. Alfaruqi, V. Mathew, J. Gim, S. Kim, J. Song, J. P. Baboo, S. H. Choi, J. Kim, *Chem. Mater.* **2015**, *27*, 3609.

[16] P. He, M. Yan, G. Zhang, R. Sun, L. Chen, Q. An, L. Mai, *Adv. Energy Mater.* **2017**, *7*, 1601920.

[17] J. H. Jo, Y.-K. Sun, S.-T. Myung, *J. Mater. Chem. A* **2017**, *5*, 8367.

[18] P. Y. Zavalij, F. Zhang, M. Whittingham, *Cryst. Struct. Commun.* **1997**, *53*, 1738.

[19] G. Yang, S. Li, M. Wu, C. Wang, *J. Mater. Chem. A* **2016**, *4*, 10974.

[20] Y. Yu, C. Niu, C. Han, K. Zhao, J. Meng, X. Xu, P. Zhang, L. Wang, Y. Wu, L. Mai, *Ind. Eng. Chem. Res.* **2016**, *55*, 2992.

[21] H. Yan, Y. Luo, X. Xu, L. He, J. Tan, Z. Li, X. Hong, P. He, L. Mai, *ACS Appl. Mater. Interfaces* **2017**, *9*, 27707.

[22] a) R. Y. Wang, C. D. Wessells, R. A. Huggins, Y. Cui, *Nano Lett.* **2013**, *13*, 5748; b) M. H. Alfaruqi, J. Gim, S. Kim, J. Song, J. Jo, S. Kim, V. Mathew, J. Kim, *J. Power Sources* **2015**, *288*, 320; c) J. Lee, J. B. Ju, W. I. Cho, B. W. Cho, S. H. Oh, *Electrochim. Acta* **2013**, *112*, 138; d) B. Lee, C. S. Yoon, H. R. Lee, K. Y. Chung, B. W. Cho, S. H. Oh, *Sci. Rep.* **2014**, *4*, 6066.

[23] H.-S. Kim, J. B. Cook, H. Lin, J. S. Ko, S. H. Tolbert, V. Ozolins, B. Dunn, *Nat. Mater.* **2017**, *16*, 454.

[24] J. Wang, J. Polleux, J. Lim, B. Dunn, *J. Phys. Chem. C* **2007**, *111*, 14925.

[25] a) K. Tang, X. Yu, J. Sun, H. Li, X. Huang, *Electrochim. Acta* **2011**, *56*, 4869; b) P. He, X. Zhang, Y.-G. Wang, L. Cheng, Y.-Y. Xia, *J. Electrochem. Soc.* **2008**, *155*, A144.

[26] X. Rui, N. Ding, J. Liu, C. Li, C. Chen, *Electrochim. Acta* **2010**, *55*, 2384.

[27] G. Wang, Q. Qu, B. Wang, Y. Shi, S. Tian, Y. Wu, R. Holze, *J. Power Sources* **2009**, *189*, 503.

[28] M.-S. Wu, M.-J. Wang, J.-J. Jow, W.-D. Yang, C.-Y. Hsieh, H.-M. Tsai, *J. Power Sources* **2008**, *185*, 1420.

[29] H. Xia, L. Lu, G. Ceder, *J. Power Sources* **2006**, *159*, 1422.

[30] Z. Liu, P. Bertram, F. Endres, *J. Solid State Electrochem.* **2017**, *21*, 2021.

[31] B. Zhang, Y. Liu, X. Wu, Y. Yang, Z. Chang, Z. Wen, Y. Wu, *Chem. Commun.* **2014**, *50*, 1209.

[32] Y.-S. Kim, W.-P. Tai, S.-J. Shu, *Thin Solid Films* **2005**, *491*, 153.

[33] H.-q. Jiang, H. Endo, H. Natori, M. Nagai, K. Kobayashi, *Mater. Res. Bull.* **2009**, *44*, 700.

1705580 (7 of 7)